

Analytical and Numerical Models Compared with Measurements for Analysis of Electromagnetic Radiation through Apertures of a Metallic Enclosure

Hakim Azizi¹, Mohammed Chebout¹, Hocine Moulai²,
Arnaud Bréard³, Christian Vollaire³

Abstract: Generally, most of the electronic equipments need a metallic enclosure in order to mechanically protect and electrically shield the interior printed circuit boards (PCBs) and subsystems. But in practical situations, the apertures or slots of various forms are essential parts of the shielding enclosure for thermal dissipation, CD-ROMs, connectors, I/O cabling and so on. The performance of shielding enclosures for high-speed digital systems is compromised by these inevitable discontinuities on enclosure. To minimize the electromagnetic interferences and susceptibility risks by these discontinuities, the shielding enclosures with apertures should be designed based on thorough analysis about the electromagnetic coupling mechanism through apertures. In this paper, the effect of apertures and oblique incident plane wave on shielding effectiveness of the enclosure is studied with the Circuital Approach, and the Finite-Difference Time-Domain (FDTD) method, the simulated SE data are verified by experimental technique. Good agreements are found between these approaches.

Keywords: Shielding Effectiveness, Enclosures, Apertures, Normal incident, Oblique incident.

1 Introduction

Recently, as the electronic industry makes remarkable progress based on the high technologies, the structure of the electronic equipments and systems including lots of chips, packages and printed circuit boards becomes more and more complex.

Accordingly, the system requirements related to the signal/power integrity or electromagnetic interferences (EMI) such as the timing budgets, the noise margin and the limits on the radiated emission are getting more and more stringent [1, 3].

¹University Ziane Achour of Djelfa; E-mails: azizihakimbilal@yahoo.fr, chebout_med@yahoo.fr

²L2EIS Laboratory, University of Sciences and Technology Houari Boumediene, Algeria;
E-mails: hmoulai@usthb.dz

³Ampere Laboratory, Central school of Lyon, France; E-mails: arnaud.breard@ec-lyon.fr,
christian.vollaire@ec-lyon.fr

As it is well known, most of the electronic equipments need a metallic enclosure for mechanically protecting and electrically shielding the interior (Printed Circuit Board "PCB") and subsystems. The metallic shielding enclosure (Fig. 1) is frequently used to reduce the emission or improve the immunity of electronic equipments. From an EMC point of view, it takes into account the effects of the apertures.

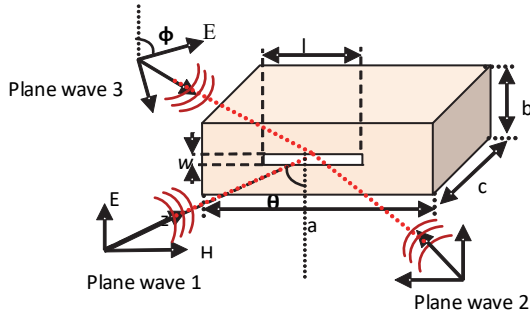


Fig. 1 – Rectangular enclosure with aperture.

The performance of a shielding enclosure is quantified by its shielding Effectiveness (SE), defined as the ratio of the field strength in the presence and absence of the enclosure. The apertures are responsible on the degradation of the performance of the enclosure. In order to minimize these risks of electromagnetic interference and susceptibility due to these discontinuities, the shield housing and apertures must be designed based on thorough analysis of the electromagnetic coupling mechanism through the apertures [4, 5].

Recently, several methods have been employed to assess the shielding effectiveness of metallic enclosures with apertures on their walls. A rigorous approach to this problem would require the solution of a complex scattering problem, taking into account the re-irradiation from the enclosure. Since a closed-form solution to this kind of problem is generally not available, numerical methods have been applied including transmission-line-matrix (TLM) method [6], finite-difference time-domain (FDTD) method [7, 10] and method of moments (MoM) [11, 12]. Although they are quite accurate, it is difficult for EMC designers to use them to investigate the effect of design parameters on shielding effectiveness during the product design stage because they are computationally intensive.

In this article, the effect of the apertures on the shielding effectiveness of the enclosure has been studied with the circuit model [1]. The quality and degree of approximation of the developed model are determined by validating the results of the modeling with those obtained by the finite difference method (FDTD) and experimental measurements.

In many practical situations, an EMC designer would prefer to have a fast, although approximate, solution to the problem in order to speed up the design process. To this end, a circuital approach was proposed, where the aperture was assumed to be a length of coplanar strip transmission line, and the enclosure was modeled as a length of a rectangular guided wave ended with a short circuit [5]. This straightforward approach is limited to centered apertures where the incident plane wave can only have one polarization direction of travel.

However, in this work, we extend Robinson's work to determine shielding effectiveness of a loaded enclosure with off-centred aperture considering the oblique incidence and polarization.

The present approach extends then this study to arbitrarily polarized incident plane waves. Fields have been calculated inside the box when a plane wave source is crossing over the rectangular enclosure. It has been shown that the fields inside the box depend on the frequency, the modal structure of the fields inside the box, the position inside the box, the angle of incidence and polarization of the incident wave. The work confirms the non-deterministic nature of the problem and privileges the statistical investigation of the SE problem.

2 The Transmission Line Model

A rectangular aperture in an empty rectangular enclosure (Fig. 1) is represented by the equivalent circuit of Robinson and *al.* [1], which is shown in Fig. 2. The longer side of the slot is shown normal to the *E*-field, which is the worst case for shielding.

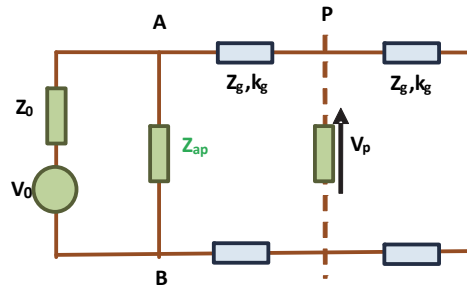


Fig. 2 – Robinson *et al.* equivalent circuit.

The electric shielding at a distance *p* from the slot is obtained from the voltage at point *P* in the equivalent circuit, while the current at *P* gives the magnetic shielding. The radiating source is represented by voltage V_0 and impedance $Z_0 = 377\Omega$ and the enclosure by the shorted waveguide whose characteristic impedance and propagation constant are Z_g and k_g .

2.1 Slot impedance

The aperture is represented as a length of coplanar strip transmission line, shorted at each end (implying that we need only to consider the transmission line currents on the front face of the enclosure). The total width is equal to the height of the enclosure b and the separation is equal to the width of the slot w . Its characteristic impedance is given by Gupta et al. [13] as $Z_{0s} = 120\pi K(w_e/b)/K'(w_e/b)$, where K and K' are elliptic integrals. The effective width w_e is given by:

$$w_e = w - \frac{5t}{4\pi} \left(1 + \ln \frac{4\pi w}{t} \right), \quad (1)$$

where t is the thickness of the enclosure wall. If $w_e < b/\sqrt{2}$ (which is true for most practical apertures) then, according to Gupta et al [13], the following approximation can be used:

$$Z_{0s} = 120\pi^2 \left[\ln \left(2 \frac{\sqrt[4]{1-(w_e/b)^2}}{\sqrt{1-\sqrt[4]{1-(w_e/b)^2}}} \right) \right]^{-1}. \quad (2)$$

To calculate the aperture impedance Z_{ap} , the short circuits at the ends of the aperture are transformed through a distance $l/2$ to the center. This is represented by point A in the equivalent circuit. It is necessary here to include a factor l/a to take into account the coupling between the aperture and the enclosure:

$$Z_{ap} = \frac{1}{2} \frac{l}{a} j Z_{0s} \tan \frac{k_0 l}{2}. \quad (3)$$

This assumption is considered for the connection between transmission line and waveguide. To calculate the aperture impedance Z_{ap} , the load impedance Z_l is transformed at the ends of the aperture through a distance $l/2$ to the center. A factor C_{mn} is introduced to take into account the high-order mode and coupling between aperture and enclosure:

$$Z_{ap} = \frac{1}{2} C_{mn} Z_{0s} \frac{Z_l + j Z_{0s} \tan(k_0 l/2)}{Z_{0s} + j Z_l \tan(k_0 l/2)}. \quad (4)$$

If there are n similar apertures in one face of the enclosure, then the individual apertures must be combined. We assume that the individual impedance may simply be combined in series, giving then total impedance:

$$Z_{ap} = \sum_n \frac{1}{2} C_{mn} Z_{0s} \frac{Z_l + j Z_{0s} \tan(k_0 l/2)}{Z_{0s} + j Z_l \tan(k_0 l/2)}. \quad (5)$$

This simple approach ignores the mutual admittance between apertures and may not be applicable if apertures are too close. [1] and [14] take enclosure as perfect conductor whose conductivity is infinite. But for practical material, its impedance should be written as:

$$Z_l = (1 + j) \sqrt{\frac{\pi f \mu_1}{\sigma_1}}, \quad (6)$$

μ_1 and σ_1 are determined by the enclosure material properties.

By assuming the aperture field is of the form:

$$E_{ap}^x = E_0 \sin \frac{m(x - x_0)\pi}{l} \cos \frac{n(y - y_0)\pi}{w} \exp[j(\omega t - k_0 z)], \quad (7)$$

where l and w are the length and width of aperture respectively.

Fig. 3 shows the coordinate system used in the rectangular waveguide formula. The electric field y-component in TE_{mn} or TM_{mn} wave is:

$$E^y = A \sin \left(\frac{m\pi x}{a} \right) \cos \left(\frac{n\pi y}{b} \right) \exp[j(\omega t - k_{mg} z)]. \quad (8)$$

According to field continuity at the aperture, the coupling coefficient C_{mn} can be obtained by the following equation:

$$C_{mn} = \frac{\int_{x_0}^{x_0+l} \int_{y_0}^{y_0+w} \cos \left(\frac{n\pi y}{b} \right) \cos \left(\frac{n(y - y_0)\pi}{w} \right) \sin \left(\frac{\pi mx}{a} \right) \sin \left(\frac{\pi(x - x_0)m}{l} \right) dx dy}{XY}, \quad (9)$$

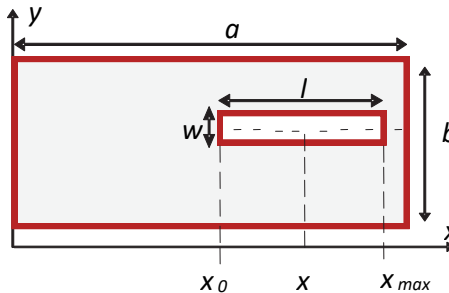


Fig. 3 – Coordinate system, X and Y are the coordinates of the aperture center.

2.2 Electric and magnetic shielding effectiveness

By applying Thevenin's theorem and combining Z_0 , V_0 and Z_{ap} , one obtains an equivalent voltage:

$$V_1 = \frac{V_0 Z_{ap}}{Z_0 + Z_{ap}} \quad (10)$$

and source impedance:

$$Z_1 = \frac{Z_0 Z_{ap}}{Z_0 + Z_{ap}}. \quad (11)$$

For the TE_{10} mode of propagation, the waveguide has characteristic impedance:

$$Z_g = \frac{Z}{\sqrt{1 - \left(\frac{\lambda}{2a}\right)^2}} \quad (12)$$

and propagation constant:

$$k_g = k \sqrt{1 - \left(\frac{\lambda}{2a}\right)^2}, \quad (13)$$

where $k = 2\pi/\lambda$, $Z = \sqrt{\mu/\epsilon}$, μ and ϵ are determined by enclosure material nature.

Note that Z_g and k_g are imaginary at frequencies below the cut-off frequency (equal to $c_0/2a$).

In addition, by transforming V_1 , Z_1 and the short circuit at the end of the waveguide to P , this gives an equivalent voltage V_2 , a source impedance Z_2 , and a load impedance Z_3 such as:

$$V_2 = \frac{V_1}{\cos k_g p + j \frac{Z_1}{Z_g} \sin k_g p}, \quad (14)$$

$$Z_2 = \frac{Z_1 + j Z_g \tan k_g p}{1 + j \frac{Z_1}{Z_g} \tan k_g p}, \quad (15)$$

$$Z_3 = Z_g \frac{Z_1 + j Z_g \tan k_g p (c - p)}{Z_g + j Z_1 \tan k_g p (c - p)}. \quad (16)$$

The voltage at P is then:

$$V_p = \frac{V_2 Z_3}{Z_2 + Z_3} \quad (17)$$

and the current at P is:

$$i_p = \frac{V_2}{Z_2 + Z_3}. \quad (18)$$

In the absence of enclosure, the load impedance at P is simply Z_0 . The voltage at P is:

$$V'_p = \frac{V_0}{2} \quad (19)$$

and the current is:

$$i'_p = \frac{V_0}{2Z_0}. \quad (20)$$

The electric and magnetic shielding are therefore given by:

$$S_E = -20 \log_{10} \left| \frac{V_p}{V'_p} \right| = -20 \log_{10} \left| \frac{2V_p}{V_0} \right|, \quad (21)$$

$$S_M = -20 \log_{10} \left| \frac{i_p}{i'_p} \right| = -20 \log_{10} \left| \frac{2i_p Z_0}{V_0} \right|. \quad (22)$$

3 S_E and S_M Formula Extensions

3.1 Equivalent admittance of an array of apertures

For array of apertures given in Fig. 4, the normalized shunt admittance is [15]:

$$\frac{Y_{ah}}{Y_0} = -j \frac{3d_h d_v \lambda_0}{\pi d^3} + j \frac{288}{\pi \lambda_0 d^2} \left[\sum_{m=0}^{\infty} \sum_{\substack{n=0 \\ m \neq odd}}^{\infty} \left(\frac{\epsilon_m n^2}{d_v^2} + \frac{\epsilon_n m^2}{d_h^2} \right) J_1^2(X) \right], \quad (23)$$

where λ_0 and Y_0 are the free-space wavelength and intrinsic admittance, respectively, d_v and d_h are the vertical and horizontal hole separations assuming that the holes' diameter d is smaller than the separations,

$$X = \frac{\sqrt{\frac{m^2}{d_h^2} + \frac{n^2}{d_v^2}}}{\sqrt{\frac{m^2}{d_h^2} + \frac{n^2}{d_v^2}}}, \quad (24)$$

J_1 is the Bessel function of the first kind of the first order, and $\epsilon_{m,n}$ if $m,n=0$ and 2 if $m,n \neq 0$.

The second term in (23) can be neglected when d_v , d_h and d are much less than the wavelength. The impedance $Z_{ah} = 1/Y_{ah}$ models the array of small holes linking the free space with the waveguide [16].

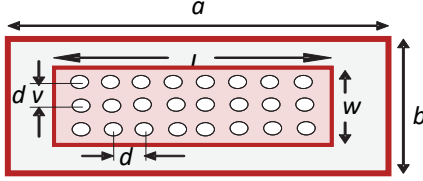


Fig. 4 – Wall of an enclosure partially perforated by a centered array of holes.

Fig. 4 depicts an enclosure wall partially perforated by an array of holes; its effective wall impedance Z'_{ah} is a fraction of Z_{ah} . By using an impedance ration concept, Z'_{ah} becomes:

$$Z'_{ah} = Z_{ah} \times \frac{(w \times l)}{(a \times b)}, \quad (25)$$

where length l and width w of the array are:

$$l = d_h/2 + (m-1) \times d_h + d_h/2, \quad (26)$$

$$w = d_v/2 + (n-1) \times d_v + d_v/2. \quad (27)$$

Here, m and n are the number of holes in length and width of the array, respectively.

For the case of an array of square holes, the same model could be applied using equivalent circles. The square holes of side d_s are replaced with equivalent encompassing circles of diameter $d = \sqrt{2}d_s$.

3.2 SE for any polarization angles and incident angles plane wave

The expressions of two electric field components are written as follows [4]:

$$E_{\perp} = E \sin \varphi, \quad (28)$$

$$E_{\parallel} = E \cos \varphi. \quad (29)$$

The transmission coefficient at the separation surface of two media is given by this expression [4]:

$$T = \frac{2Z'_2}{Z'_2 + Z'_1}, \quad (30)$$

where Z'_1 is the impedance of the air and Z'_2 is the impedance of the aperture.

The ratio of the propagation constants and that of the intrinsic impedances as follows [4]:

$$\frac{k_1}{k_2} = \sqrt{\frac{\epsilon_1}{\epsilon_2}}, \quad (31)$$

$$\frac{Z_0}{Z_{ap}} = \sqrt{\frac{\epsilon_2}{\epsilon_1}}. \quad (32)$$

According to Snell's law:

$$\sin \theta_T = \sqrt{\frac{\epsilon_1}{\epsilon_2}} \sin \theta_i. \quad (33)$$

We suppose that [4]:

$$Z'_2 = Z_{ap} / \cos \theta_T, \quad (34)$$

$$Z'_1 = Z_0 / \cos \theta_i, \quad (35)$$

θ_i is the angle of incidence, θ_T is the angle of transmission,

We can therefore calculate the field component for this polarization via the following expression [4]:

$$E_\perp^1 = T_\perp E_\perp. \quad (36)$$

We substitute V_1 by E_\perp^1 in relation (14), we obtain the following formula:

$$V_2 = \frac{E_\perp^1}{\cos k_g p + j(Z_1/Z_g) \sin k_g p}. \quad (37)$$

To calculate the transmission coefficient of the parallel polarization, the following two quantities are assumed [4]:

$$Z'_2 = Z_{ap} \cos \theta_T, \quad (38)$$

$$Z'_1 = Z_0 \cos \theta_i. \quad (39)$$

In order to find the value of T_\parallel , one must follow the same sequence described previously concerning T_\perp

$$E_\parallel^1 = T_\parallel E_\parallel. \quad (40)$$

We substitute in relation (37) [4], we obtain the tension as follows:

$$V_3 = \frac{E_\parallel^1}{\cos k_g p + j(Z_1/Z_g) \sin k_g p}. \quad (41)$$

After studying each case separately, we calculate the equivalent voltages in a point for the two polarization cases by means of two expressions:

$$V_{p\perp} = \frac{V_2 Z_3}{Z_2 + Z_3}, \quad (42)$$

$$V_{p\parallel} = \frac{V_3 Z_3}{Z_2 + Z_3}. \quad (43)$$

The superposition is carried out by means of this formula [4]:

$$V_p = \sqrt{(V_{p\perp})^2 + (V_{p\parallel})^2}. \quad (44)$$

4 FDTD Modeling

The FDTD method has been widely applied to solving different types of electromagnetic scattering problems [7, 10]. It possesses the advantages of simple implementation for relatively complex problems, high accuracy and the ability of work with a wide range of frequencies, stimuli, objects, environments and response locations. A disadvantage of the FDTD method is linked to the time domain formulation where computations on resonant structures lead to prohibitively long computation times and that significant computational resources are expended for modeling an electrically small object without the aid of special sub cellular or multi grid algorithms.

Calculations performed by the FDTD method are defined by specifying dielectric and magnetic material parameters at the calculated electric and magnetic field locations. This method is based on the discretization of Maxwell's two curl equations directly in time and spatial domains and dividing the volume of interest into unit (Yee) cells [5, 18]. These equations in loss regions with sources can be written as:

$$\frac{\partial \vec{E}}{\partial t} = \frac{1}{\epsilon} \left[\nabla \times \vec{H} - \sigma \vec{E} \right], \quad (45)$$

$$\frac{\partial \vec{H}}{\partial t} = -\frac{1}{\mu} \left[\nabla \times \vec{E} - \rho' \vec{H} \right], \quad (46)$$

where:

$$\vec{B} = \mu \vec{H}, \quad (47)$$

$$\vec{D} = \epsilon \vec{E}, \quad (48)$$

$$\vec{J}_e = \sigma \vec{E}, \quad (49)$$

$$\vec{J}_m = \rho' \vec{H}, \quad (50)$$

where ρ' is a term of magnetic losses (Ω/m), \vec{B} , \vec{D} , \vec{E} , \vec{H} , \vec{J}_m , \vec{J}_e are the magnetic flux density, electric flux density, electric field, magnetic field, induced magnetic current density, and impressed electric current density vectors, respectively.

FDTD technique uses simple central-difference approximations to evaluate the space and time derivatives. It consists of a time stepping procedure. Inputs are time-sampled analog signals. The region being modeled is represented by two interleaved grids of discrete points (Fig. 5).

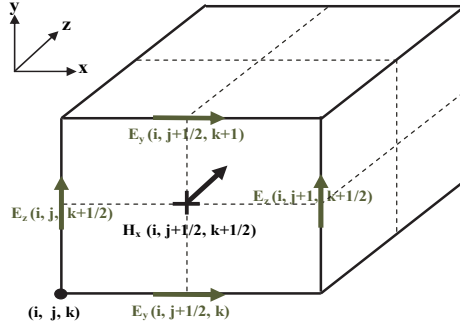


Fig. 5 – Positions of the field components in Yee cell unit.

By staggering the discrete electric and magnetic fields in space and time, this leads to a second order accurate approximation, from which an explicit update scheme can be derived. For example, the explicit update expression for E_x is:

$$\begin{aligned} E_{x(i+1/2, j, k)}^{n+1} = & Ca_{(i+1/2, j, k)} E_{x(i+1/2, j, k)}^n + \\ & + \frac{Cb_{(i+1/2, j, k)}}{\Delta y} [H_{z(i+1/2, j+1/2, k)}^{n+1/2} - H_{z(i+1/2, j-1/2, k)}^{n+1/2}] + \\ & + \frac{Cb_{(i+1/2, j, k)}}{\Delta z} [H_{y(i+1/2, j, k-1/2)}^{n+1/2} - H_{y(i+1/2, j, k+1/2)}^{n+1/2}], \end{aligned} \quad (51)$$

where:

$$Ca_{(i, j, k)} = \frac{1 - \frac{\sigma_{(i, j, k)} \Delta t}{2\epsilon_{(i, j, k)}}}{1 + \frac{\sigma_{(i, j, k)} \Delta t}{2\epsilon_{(i, j, k)}}}, \quad (52)$$

$$Cb_{(i, j, k)} = \frac{\frac{\Delta t}{\epsilon_{(i, j, k)}}}{1 + \frac{\sigma_{(i, j, k)} \Delta t}{2\epsilon_{(i, j, k)}}}. \quad (53)$$

The spatial increments in the x , y , and z directions are

$$\Delta x = \Delta y = \Delta z = 10.8 \text{ mm} .$$

The time step associated with this spatial increment dimension is:

$$\Delta t = \frac{\Delta x}{2 \times c} = \frac{0.0108}{2 \times (3 \times 10^8)} = 1.8 \times 10^{-11} \text{ s} . \quad (54)$$

The simulations typically required are from 11000 to 14000 time steps to achieve the steady state. The simulation was carried out on a 4 GB memory computer with a processor of 3.66 GHz speed running for 8 hours. Hamming windowing was used to smooth the obtained data before Fourier transform was applied to the data to obtain frequency-domain information.

5 Measurement Setup

The Shielding Effectiveness of the enclosure with aperture has been measured on an aluminium cube with a thickness of 2 mm. Five walls of the cube are carefully welded together. This ensures that no leakage penetrates these parts of the box, and the sixth wall contains a rectangular aperture.

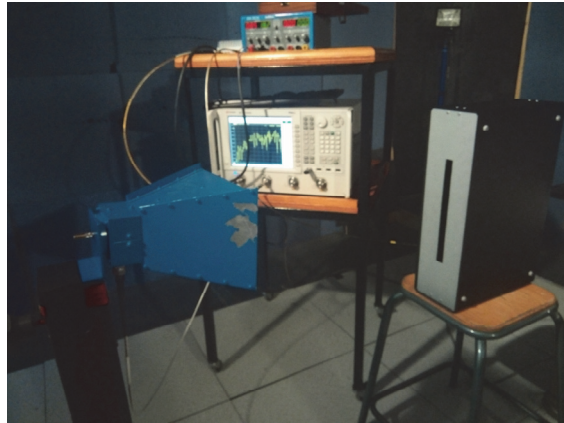


Fig. 6 – Measuring bench in semi-anechoic room.

The measurements are performed in an anechoic chamber as shown in Fig. 6, where, with the exception of the conducting ground, the walls are covered with absorbents (ferrite tile associated with laminated absorbents). A horn antenna is used as a transmitting antenna at a frequency range of 200 MHz – 18 GHz (Fig. 6). The receiving antenna is placed in the center of the enclosure. We also used a Vector Network Analyzer (VNA) that allows characterizing quadrupoles in frequency domain (between 300 kHz and 8 GHz). SE Results are based on the S parameters measurement. The transmitting antenna is connected to the VNA and a Near Field Probe Set DC to 9 GHz (Isotropic E-field probe) is used as a receiving antenna at a frequency range of 1 Hz – 9 GHz that is connected to

a coaxial bushing connector High quality special SMB to SMA; cable for connecting any Probe with various test equipment and the output of the connector is connected to the VNA.

6 Results and Discussions

6.1 Geometry of the tested enclosure

The tested rectangular enclosure of $(134 \times 474 \times 300) \text{ mm}^3$ dimensions with a $(20 \times 250) \text{ mm}^2$ aperture is shown in Fig. 6. The electric and magnetic shielding at a distance p from the slot is obtained from the electric and magnetic fields at point P .

In this paper, SE is calculated in the center of the enclosures and the effect of some parameters such as polarization and aperture are taken into account [19, 20].

6.2 Definition of shielding effectiveness

Shielding Effectiveness (SE) is used to assess the effect of shielding in electromagnetic coupling problems of cavities with apertures. The definition of SE is based on a plane wave excitation and the following procedure [4, 5] (numerical, experimental way):

- Excite the cavity with an incident pulse plane wave and record the electric field at the position of interest.
- Excite an empty space computational domain with the same incident pulse plane wave and record the electric field at the position of interest.
- Fourier transform of the time-domain data.
- Compute the SE in decibels

SE is defined as the ratio of electric fields and SM of magnetic fields such as:

$$SE = 20 \log \frac{E_{y0}}{E_{y1}}, \quad (55)$$

$$SM = 20 \log \frac{H_{x0}}{H_{x1}}, \quad (56)$$

where E_{y0} and H_{x0} : the electric and magnetic field strength with the shield, E_{y1} , H_{x1} : the electric field strength in the absence of the shield

6.3 Validation of the results

Fig. 7 shows the shielding effectiveness calculated (FDTD and analytical) and measured in the center of enclosure of dimensions $(134 \times 474 \times 300) \text{ mm}^3$ with a $(20 \times 250) \text{ mm}^2$ aperture. The calculations as well as the measurements show the fundamental resonance frequency at around 1.24 GHz. There is a good agreement between the different results obtained.

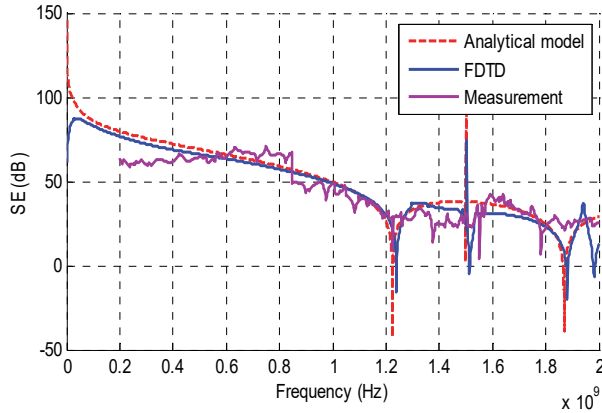


Fig. 7 – Comparison between computed (FDTD), modeled (analytical) and measured (VNA) SE.

6.4 SE for distinct positions of the enclosure

In this study, we use our extended Robinson model to evaluate the SE for two distinct positions of the enclosure: the first one is chosen in such a way the enclosure is horizontal of dimension $(474 \times 134 \times 300)$ mm 3 with a (250×20) mm 2 aperture; the second one is for a vertical enclosure of dimension $(134 \times 474 \times 300)$ mm 3 with a (20×250) mm 2 aperture.

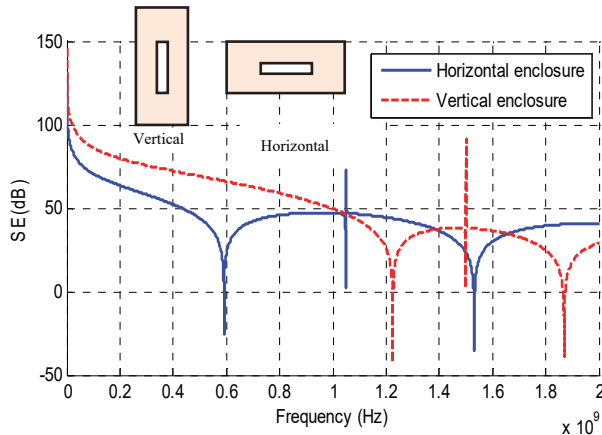


Fig. 8 – SE for two boxes of the same dimensions and two different positions.

One can conclude that the shielding effectiveness of a vertical enclosure is better than a horizontal enclosure (Fig. 8).

During this study, we focused on the case of an enclosure and aperture with a vertical position.

6.5 Electric Shielding Effectiveness for three positions according to Z direction

We next proceed to examine the *SE* an enclosure of dimension $(134 \times 474 \times 300) \text{ mm}^3$ with our extended Robinson model at different points (P_0 , P_1 , P_2).

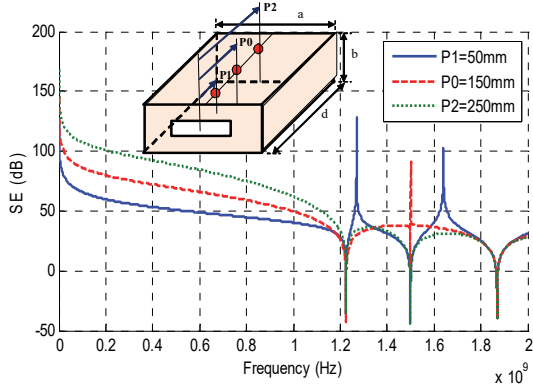


Fig. 9 – Calculated SE at three positions (P_z).

Fig. 9 shows the calculated *SE* at different sampling points ($P_z = P_0, P_1, P_2$) within the unloaded $(134 \times 474 \times 300) \text{ mm}^3$ enclosure with a $(20 \times 250) \text{ mm}^2$ aperture. The calculations show that the enclosure resonates at approximately 1.24 GHz, leading to negative shielding (field enhancement) around this frequency. Below the resonance frequency, *SE* decreases with frequency and increases with distance from the aperture.

6.6 SE of the same aperture at different positions

Fig. 10 shows the *SE* of the same aperture at different positions.

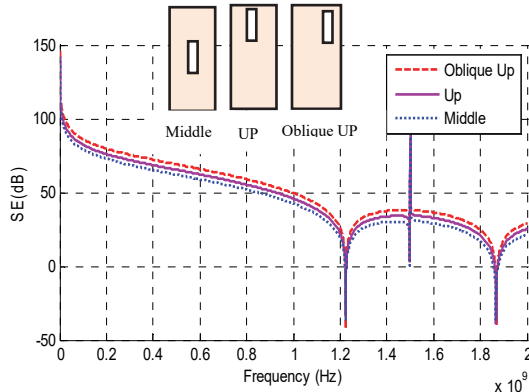


Fig. 10 – SE in three cases.

In general, the *SE* of middle aperture is the worst. The nearer the aperture is to the edge, the better The *SE* is. Based on the results, electronic engineers should place apertures at the edge positions of the shielding box.

6.7 Rectangular enclosure with numerous apertures

Fig. 11 depicts the *SE* results for the same enclosure configurations ($134 \times 474 \times 300$ mm 3) but with different numbers of apertures (2×2), (4×4) and (6×6) ($d_v = 68\text{mm}$, $d_h = 20\text{mm}$). In each case, the total area was 51cm^2 .

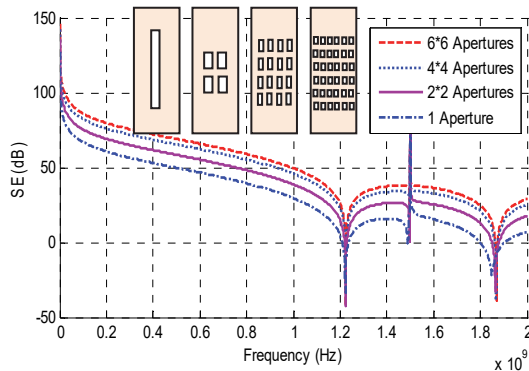


Fig. 11 – Electrical *SE* results for the same enclosure configurations, but with different arrays of (2×2), (4×4) and (6×6).

The analytical solution predicts that *SE* is increased by increasing the number of apertures while keeping the same total area (Fig. 11).

6.8 Change of *SE* by arbitrary angle of polarization

Fig. 12 shows calculated *SE* with polarization angle.

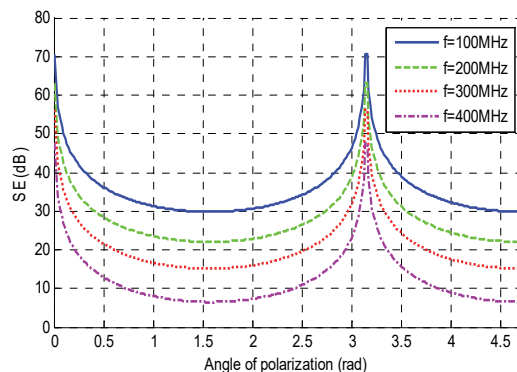


Fig. 12 – Shielding effectiveness by plane wave of arbitrary angle of polarization.

It can be seen that the shielding coefficient decreases when the polarization angle is in the range of $0 < \psi < \pi/2$ and increases in $\pi/2 < \psi < \pi$. And shielding effectiveness of low frequency is better than that of high frequency.

7 Conclusion

The electromagnetic coupling into a rectangular enclosure with aperture has been investigated using the transmission-line model. Estimation of the shielding effectiveness based on the multimode approach offers a cost-effective alternative to the FDTD technique, saving significant computing resources and experimental techniques. Good agreement is found between the results obtained from these techniques.

In this work, an efficient analytical approach based on the equivalent circuit model of a waveguide has been developed to calculate the *SE* of open metal enclosures (the Robinson method in the present case), made it possible to study the various parameters involved in the design of electromagnetic shielding housings. Among the advantages of the analytical model, we mention the speed of calculation and the simplicity of implementation. For these reasons, this method is preferred by electromagnetic shielding designers.

8 References

- [1] M.P. Robinson, T.M. Benson, C. Christopoulos, J.F. Dawson, M. D. Ganley, A.C. Marvin, S.J. Porter, D.W.P. Thomas: Analytic Formulation for the Shielding Effectiveness of Enclosure with Apertures, IEEE Transactions on Electromagnetic Compatibility, Vol. 40, No. 3, August 1998, pp. 240 – 248.
- [2] S. Yenikaya: Electromagnetic Analysis and Shielding Effectiveness of Rectangular Enclosures with Aperture using Hybrid MoM/FEM, Iranian Journal of Electrical and Computer Engineering (IJECE), Vol. 10, No. 2, June 2011, pp. 70 – 76.
- [3] A. Rabat, P. Bonnet, K. El Khamlichi Drissi, S. Girard : Analytical Formulation for Shielding Effectiveness of a Lossy Enclosure Containing Apertures, IEEE Transactions on Electromagnetic Compatibility, Vol. 60, No. 5 , October 2018, pp. 1384 – 1392.
- [4] D. Shi, Y. Shen, F. Ruan, Z. Wei, Y. Gao: Shielding Analysis of Enclosure with Aperture Irradiated by Plane Wave with Arbitrary Incident Angle and Polarization Direction, Proceedings of the IEEE International Symposium on Electromagnetic Compatibility, Detroit, USA, August 2008, pp. 1 – 5.
- [5] H. Azizi, F.T. Belkacem, D. Moussaoui, M. Bensetti: Numerical Study for the Shielding Effectiveness of a Rectangular Enclosure with Apertures, International Symposium on Electromagnetic Compatibility -EMC EUROPE, Roma, Italy, September 2012, pp. 1 – 6.
- [6] B.-L. Nie, P.-A. Du: Electromagnetic Shielding Performance of Highly Resonant Enclosures by a Combination of the FETD and Extended Prony's Method, IEEE Transactions on Electromagnetic Compatibility, Vol. 56, No. 2, April 2014, pp. 320 – 327.
- [7] X. Gao, L. Kong: The Application of Improved FDTD Algorithm Based on Mode-Matching in Shielding Cavity, Proceedings of the 2nd International Conference on Electronic Information Technology and Computer Engineering (EITCE 2018), Shanghai, China, October 2018, pp. 1 – 3.

- [8] K.- P. Ma, M. Li, J. L. Drewniak, T. H. Hubing, T. P. Van Doren: Comparison of FDTD Algorithms for Subcellular Modeling of Slots in Shielding Enclosures, IEEE Transactions on Electromagnetic Compatibility, Vol. 39, No. 2, May 1997, pp. 147 – 155.
- [9] C. Jiao, L.Li, X. Cui, H.Li: Subcell FDTD Analysis of Shielding Effectiveness of a Thin-Walled Enclosure with an Aperture, IEEE Transactions on Magnetics, Vol. 42, No. 4, April 2006, pp. 1075 – 1078.
- [10] Z. Liu,Y. Li, Z. Pan, Y. Su, X. Wang: FDTD Computation of Shielding Effectiveness of Electromagnetic Shielding Fabric based on Weave Region, Journal of Electromagnetic Waves and Applications, Vol. 31, No. 3, January 2017, pp. 309 – 322.
- [11] C. Zhou, L. Tong: Study of Shielding Properties of a Rectangular Enclosure with Apertures Having Different Shapes but Same Area Using Modal Method of Moments, Research Journal of Applied Sciences, Engineering and Technology, Vol. 5, No. 2, , pp. 680 – 688.
- [12] P. Dehkoda, A. Tavakoli, M. Azadifar: Shielding Effectiveness of an Enclosure with Finite Wall Thickness and Perforated Opposing Walls at Oblique Incidence and Arbitrary Polarization by GMMoM, IEEE Transactions on Electromagnetic Compatibility, Vol. 54, No. 4, August 2012, pp. 792 – 805.
- [13] K.C. Gupta, R. Garg, I.J. Bahl: Microstrip Lines and Slotlines, 1st Edition, Artech House, Norwood, MA, 1979.
- [14] S. Dan, Y. Shen, Y. Gao: 3 High-order Mode Transmission Line Model of Enclosure with Off-center Aperture, Proceedings of the International Symposium on Electromagnetic Compatibility, Qingdao, China, October 2007, pp. 361 – 364.
- [15] T.Y. Otoshi: A Study of Microwave Leakage through Perforated Flat Plates, IEEE Transactions on Microwave Theory and Techniques, Vol. 20, No. 3, March 1972, pp. 235 – 236.
- [16] P. Dehkoda, A. Tavakoli, R. Moini: An Efficient and Reliable Shielding Effectiveness Evaluation of a Rectangular Enclosure with Numerous Apertures, IEEE Transactions on Electromagnetic Compatibility, Vol. 50, No. 1, February 2008, pp. 208 – 212.
- [17] J. Shim, D.G. Kam, J.H. Kwon, J. Kim: Circuit Modeling and Measurement of Shielding Effectiveness Against Oblique Incident Plane Wave on Apertures in Multiple Sides of Rectangular Enclosure, IEEE Transactions on Electromagnetic Compatibility, Vol. 52, No. 3, August 2010, pp. 566 – 577.
- [18] A. Taflove, K.R. Umashankar, B. Beker, F. Harfoush, K.S. Yee: Detailed FD-TD Analysis of Electromagnetic Fields Penetrating Narrow Slots and Lapped Joints in Thick Conducting Screens, IEEE Transactions on Antennas and Propagation., Vol. 36, No. 2, February 1988, pp. 247 – 257.
- [19] Q. Wang, E. Cheng, Z. Qu: On the Shielding Effectiveness of Small-Dimension Enclosures Using a Reverberation Chamber, IEEE Transactions on Electromagnetic Compatibility, Vol. 53, No. 3, August 2011, pp. 562 – 569.
- [20] Z. Liu, X.C. Wang: Influence of Fabric Weave Type on the Effectiveness of Electromagnetic Shielding Woven Fabric, Journal of Electromagnetic Waves and Applications, Vol. 26, No. 14-15, August 2012, pp. 1848 – 1856.
- [21] J.K. Park, J.N. Lee, D.H. Shin, H.J. Eom: A Full-Wave Analysis of a Coaxial Waveguide Slot Bridge using the Fourier Transform Technique, Journal of Electromagnetic Waves and Applications, Vol. 20, No. 2, January 2006, pp. 143 – 158.
- [22] J.-P. Berenger: Perfectly Matched Layer for the FDTD Solution of Wave-Structure Interaction Problems, IEEE Transactions on Antennas and Propagation, Vol. 44, No. 1, January 1996, pp. 110 – 117.